Active Control of Aerofoil Flutter

X. Y. Huang*
University of Cambridge, Cambridge, England

This paper describes a novel method of eliminating aerofoil flutter by an active control technique. The control is attained by adding to the natural case a control-induced force of appropriate amplitude and phase to negate the natural destabilizing tendency of the aerodynamic load. This control force may be induced on wings by actuating tabs or ailerons, however the present paper concentrates on a scheme that may be more effective at high frequencies and which might, therefore, complement more conventional methods. Acoustic equipment is used to carry out the techniques of active sound control that are known as anti-sound. Although loudspeaker-induced pressures are small it is shown that they can actually induce significant and useful control forces on an aerofoil. This technique offers new flexibility in system design because the loudspeakers can be positioned at a convenient place, not necessarily on the aerofoil surface. This paper describes the theory needed to assess the details of this idea and also contains the results of the experiments in which a fluttering aerofoil was stabilized by switching on a loudspeaker.

Nomenclature

A = aerodynamic matrix
a = distance from the source to the wing, see Fig. 3b
B = mass matrix
b = half-chord of the wing
C = control law matrix
c_0 = sound speed
E = stiffness matrix
F = the force exerted by a mechanical system on its surroundings
F_A = aerodynamic force
F_C = control force
G = Green function
g = gain of feedback loop
H = Hermitian matrix defined by Eq. (5)
J = function defined in Eq. (A6)
L = linear differential operator
P = rate at which work is done by the system to its surroundings
$\bar{p}$ = work done by the system in one period
Q = response matrix of a mechanical system.
Q_0 = amplitude matrix, $Q = Q_0 e^{i\omega t}$
q_i = ith generalized coordinate describing a mechanical system
R = radius of the piston or the loudspeaker
r = half-width of the strip source, see Fig. A3
S = area of piston surface
T = transfer function matrix defined in Eq. (2)
u = piston velocity
V = wind speed
α = $bJ/(1+\sqrt{1-J^2})$
σ = R/b
β = aerodynamic force coefficient
ϵ = a/b
ζ = diaphragm displacement of the piston or the loudspeaker
λ_i = ith eigenvalue of the matrix H
Π, Π_0 = source strength
ρ_0 = air density
ω = oscillation frequency
χ = displacement of the wing in bending

Superscripts

$(\ )^*$ = conjugate
$(\ )^T$ = transposition
$(\dddot{\ })$ = d^2/dt^2

I. Introduction

THE last decade has seen the development of active techniques for flutter control.[1-4] Successful control has been achieved by the use of control surfaces deflected by mechanical actuators, responding to a feedback signal. In this way, the effective aerodynamic characteristics of the aerofoil are altered, preventing the onset of flutter instability.

Nissim[5] described the general energy principle from which the condition for flutter suppression follows: for all stable oscillatory motions of an elastic system in an airstream, positive work must be done by the system on the surrounding medium. His detailed theory also shows that work can be influenced by the alteration of the aerodynamic properties of the aerofoil. Based on Nissim's theory, Sandford et al.[6] have carried out a successful experiment that demonstrated the scope of active flutter suppression on a delta wing.

Hydraulic actuators are best suited to low-frequency motion. However, Noll[2] pointed out the serious technical difficulties that arise in real flight situations where rapid response may be required. Herein a scheme is pursued that might have advantages at high frequency and incorporate some of the techniques used in anti-sound. Ffowcs Williams[7] has emphasized the principle that any unsteady linear field that can be monitored, processed, and simulated by a secondary unsteady field is amenable to active control and modification. Since conventional actuators respond sluggishly to rapid unsteady motion, they are not ideal as a means of high-frequency control, and there is, therefore, scope for more effective rapid response system capable of responding at acoustic frequencies. Here we demonstrate both experimentally and theoretically that flutter may be ac-

Received March 12, 1986; revision received Nov. 7, 1986.

*Postgraduate Student, Department of Engineering.

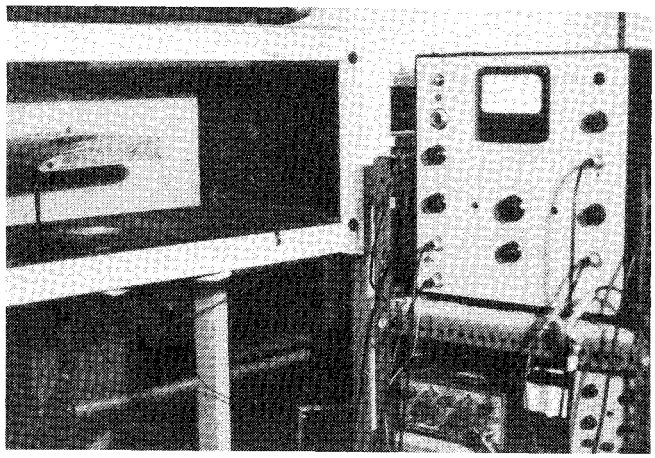

Fig. 1a Photograph of experimental devices.

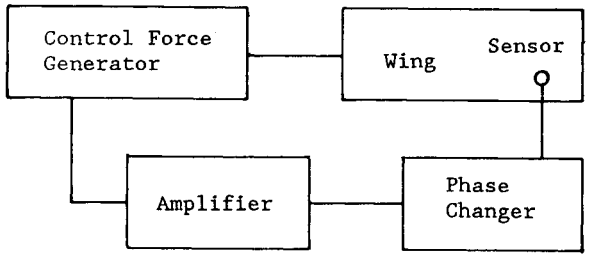

Fig. 1b Block diagram of the flutter control system.

tively controlled by the disturbance created with conventional acoustic equipment.

II. Theory of Flutter Control

We follow Nissim[5] in considering a linear mechanical system in which the force $F(t)$ exerted by the system on its surroundings at time t depends only on the immediate state of the system. If $q_i(t)$, $i=1,...n$, are the generalized coordinates describing the state of an n degree-of-freedom system, then we can write

$$F(t)=L[q_1(t),...,q_n(t)] \tag{1}$$

where L is a linear differential operator.

Let $Q=Q_0e^{i\omega t}$ be the column matrix whose entries are $q_i(t)$. Equation (1) can then be expressed in terms of a transfer function matrix T as

$$F=TQ_0e^{i\omega t} \tag{2}$$

The rate at which work is done by the mechanical system on the surroundings is

$$P=[Re(\dot{Q})]^TRe(F)$$

$$=\frac{i\omega}{4}(Q_0^TTQ_0e^{i2\omega t}-Q_0^{*T}TQ_0+Q_0^TT^*Q_0^*-Q_0^{*T}T^*Q_0^*e^{i2\omega t}) \tag{3}$$

where Q_0^{*T} denotes the conjugate transposition of the matrix Q_0. The total power output in one period is therefore

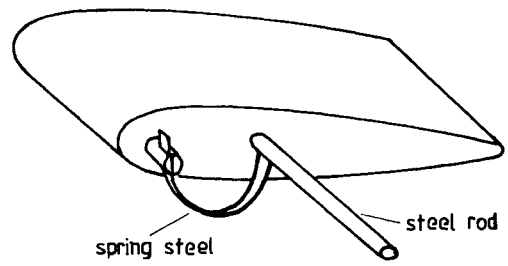

Fig. 2 The model of the wing used in the experiments.

$$\bar{P}=\frac{\pi}{2}i(Q_0^TT^*Q_0^*-Q_0^{*T}TQ_0)=\frac{\pi}{2}Q_0^{*T}HQ_0 \tag{4}$$

where

$$H=i(T^{*T}-T) \tag{5}$$

is a Hermitian matrix. A simple coordinate transformation $Q_0=UY$ allows a diagonal matrix representation of $\bar{P}$:

$$\bar{P}=\frac{\pi}{2}Y^{*T}U^{*T}HUY=\frac{\pi}{2}Y^{*T}DY$$

$$=\frac{\pi}{2}\sum\lambda_i|y_i|^2 \tag{6}$$

where D is a diagonal matrix whose entries are λ_i.

Governed by the eigenvalue λ_i of H, $\bar{P}$ is of critical importance. If it is positive, it indicates that the system will be stable, as energy is always transferred outwards. If it is negative, then any motion of the system will draw energy from outside, and the disturbance will grow.

For an aerofoil, the transfer function matrix is

$$T=-\omega^2[B+A]+E \tag{7}$$

where A is the aerodynamic matrix, B the mass matrix, and E the stiffness matrix. It follows from Eq. (5) that

$$H=-\omega^2i(B^{*T}+A^{*T}-B-A)$$

$$+i(E^{*T}-E)=-\omega^2i(A^{*T}-A) \tag{8}$$

since both B and E are symmetric.

This is the result upon which active flutter control is based. Altering the aerodynamic properties of the fluttering aerofoil may lead to a sufficient change in the eigenvalues of H such $\bar{P}$ becomes positive. Of course there are practical limitations on changing A by altering the structure of the aerofoil, and alternative strategies might offer some advantages. Such an alternative control mechanism is now proposed. The monitoring of the motion of the system and the creation of a response-related control force by nonaerodynamic means will alter the system stability; e.g., accelerations $\ddot{q}_i(t)$ might be measured and their signals processed and used to produce a control force on the aerofoil. Equation (1) can be extended to include this possiblity by writing

$$F(t)=L[q_1(t),...q_n(t)]+C[\ddot{q}_1(t),...\ddot{q}_n(t)] \tag{9}$$

where the operator C represents the control law. From Eq. (2),

$$T=-\omega^2[B+(A+C)]+E \tag{10}$$

Adding an external control force has the same effect as altering matrix A. Now

$$H = -\omega^2 i[A^{*T} - A + C^{*T} - C] \tag{11}$$

and we have more choice for changing the matrix H than was available to the designer confined to modifications of the aerodynamic matrix.

A simplified mathematical model is developed in the appendix to show that a loudspeaker (considered as a piston), either mounted on the aerofoil (considered as an unlimited strip) or remotely mounted, can supply the control forces; experiments described in the next section prove the concept.

The power flow in the system depends upon the detailed setup. In some situations the controller may prevent the aerofoil from absorbing energy from the airstream, but in others it may function as an energy absorber or even a producer of energy. The energy balance, involving as it does quadratic terms, is not the simple superposition of power flow from the aerofoil and controller acting independently.

III. Experiments of Flutter Control

Description of the Experiments

The experimental device is illustrated in Fig. 1a. The control system (Fig. 1b), consisted of a sensor, phase changer, signal amplifier, and control force generator. All experiments were carried out in a low-speed wind tunnel with a test section of 25 cm × 35 cm and a maximum speed of 20 m/s.

Figure 2 shows the type of model wing used in the experiments. The steel rod and spring steel provided a reaction to bending and torsion respectively. These were adjusted so that flutter occurred for a flow rate in the middle operating range of the wind tunnel at a frequency of 6 Hz.

The sensor is a an accelerometer that measures bending acceleration. The phase changer produces a phase shift of the feedback signal, which could be adjusted during the experiments.

The control force generator was a loudspeaker initially mounted within the wing (Fig. 3a) but finally in the wall of the wind tunnel adjacent to the wing (Fig. 3b). In this way an acoustic control force was induced on the wing.

In the case of Fig. 3a, the force generated by the loudspeaker on the wing is approximately [see Appendix, Eq. (A18b)]

$$F_C = -\pi\rho_0\omega^2 bR^2\zeta \qquad R/b < 0.5 \tag{12}$$

where ζ is the diaphragm displacement, R the radius of the loudspeaker, b the half-chord of the wing, and ρ_0 the air density. In the experiments, $b = 12.5$ cm and $R/b \simeq 0.3$.

A similar mathematical model was used for the remotely mounted loudspeaker illustrated in Fig. 3b. The loudspeaker induced control force F_C is approximately given by [see Appendix, Eq. (A20)]

$$F_C = -\pi\rho_0\omega^2 R^2\zeta\alpha \tag{13}$$

where α is given in the Appendix and depends on the ratio of b to a, the relative distance form the loudspeaker to the wing. In the experiments, $a/b \simeq 0.9$ and $R/b \simeq 0.3$.

According to Eqs. (12) and (13), the loudspeaker, which is usually regarded as a weak force generator, can actually induce large wing forces when b, the dimension of the wing, is large. The force tends to be amplified above the loudspeaker driving force by a factor proportional to the ratio of wing-to-loudspeaker dimension. This may be seen clearly through a simple example. Consider a small circular piston of area S, baffled by an infinite plane surface. If the piston velocity is $u = u_0 e^{i\omega t}$ and the wavelength $c_0/\omega \gg \sqrt{S}$, then a large force is produced on the plane surface by a piston generating only a

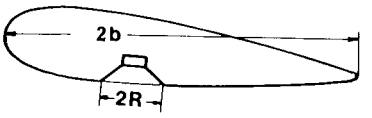

Fig. 3a Loudspeaker mounted within the wing.

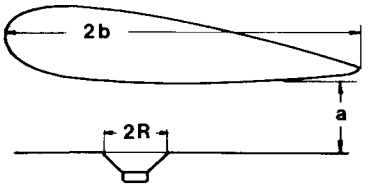

Fig. 3b Loudspeaker mounted in the wall of the wind tunnel.

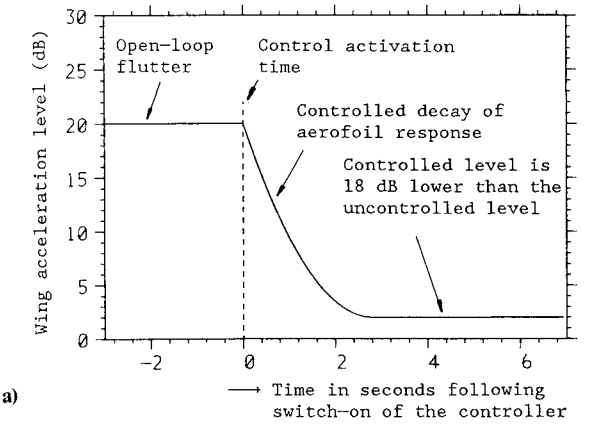

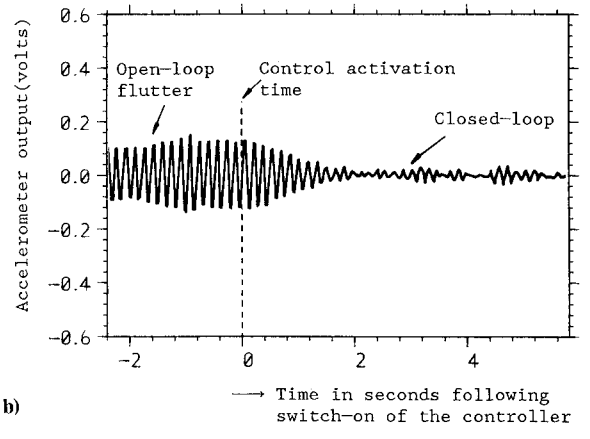

Fig. 4 Performance of the controller with loudspeaker installed in the aerofoil. The dotted lines represent the time when the controller was activated. a) Conditionally averaged trace of the rms bending acceleration of the wing; b) Typical individual time history trace of the bending acceleration of the wing.

weak pressure perturbation. The force on the plane surface is

$$F_s = \frac{\rho_0 i\omega u}{2\pi}\int_\infty \int_s \left[\frac{1}{|r-r_1|}\exp\right] - i\frac{\omega}{c_0}|r-r_1|\Big]\,dr_1\,dr$$
$$= \rho_0 c_0 S u$$

where c_0 is the sound speed, ρ_0 the air density, and r and r_1 two-dimensional vectors on the infinite plane surface and piston surface respectively. In the condition of $c_0/\omega \gg \sqrt{S}$, the force on the piston surface is[8]

$$F_p \simeq -i\frac{8}{3\pi}\rho_0\omega u S\sqrt{S}$$

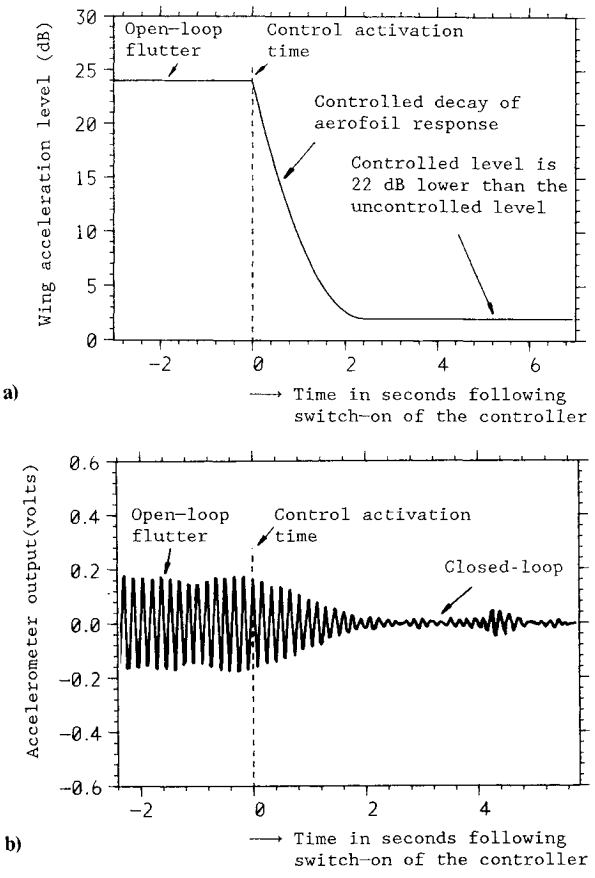

Fig. 5 Performance of the controller with loudspeaker mounted in the wall of the wind tunnel. The dotted lines represent the time when the controller was activated. a) Conditionally averaged trace of the rms bending acceleration of the wing; b) Typical individual time history trace of the bending accleration of the wing.

So that $|F_s/F_p| \simeq c_0/(\omega\sqrt{S})$, the parameter that we have assumed to be large. This amplification of the piston force is akin to but not as strong as a static hydraulic force that is induced on a surface and is bigger than the piston force by the area ratio, the linear scale squared.

The aerodynamic force on a fluttering wing can be written as

$$F_A = \beta\rho_0 V^2 b\chi \tag{14}$$

where V is the wind speed, b the half-chord, χ the displacement of the wing in bending, and β a constant. For the purpose of flutter control, the control forces should be of the same order of magnitude as the aerodynamic forces, i.e.,

$$|F_C/F_A| \sim 1 \tag{15}$$

Taking Eq. (12) for the control force, we find that

$$|F_C/F_A| = (\pi/\beta)(\omega b/V)^2(R/b)^2(\zeta/\chi) \tag{16}$$

The force generator is driven by the feedback signal, so that $\zeta = g\chi$ where g is the gain of the feedback loop. Then

$$|F_C/F_A| = (\pi/\beta)(\omega b/V)^2(R/b)^2 g \tag{17}$$

Equation (15) can be met by a suitable choice of g and R according to Eq. (17), and the acoustic term appears to offer a clear advantage at high values of reduced frequency.

Results and Discussion

During the open-loop tests, the operating speed of the wind tunnel was arranged to be just above the critical speed for flutter to occur. The performance of the controller was assessed by setting the aerofoil fluttering and then closing the control loop. Meanwhile, the phase and the amplification were adjusted until the flutter reduced. In each case, the rms bending acceleration was recorded with a level recorder (B&K Type 2306), and the time history trace of bending acceleration was plotted. The conditionally averaged root-mean-square response levels following the application of the control are given in Figs. (4) and (5).

Figure 4 shows the performance of the system with the loudspeaker installed in the aerofoil. The open-loop flutter is shown on the left side and the closed-loop operation is shown on the right side. The controller can clearly be seen to cause the unsteady flutter to decay to an insignificant level. It was found that when the flutter amplitude was small, the acoustic device performed well as a flutter controller. However, if the flutter amplitude was large, the control was ineffective, as the control force generated by the loudspeaker was amplitude limited and became weak (and nonlinear) compared with the aerodynamic forces then at work.

Figure 5 shows the performance of the system with the loudspeaker positioned in the wall of the wind tunnel as shown in Fig. 3b. The controller had a similar effect to the previous case.

IV. Conclusions

Active flutter control is a real effect that can be achieved by several different techniques. Some involve changing the aerofoil forces by convenient devices, i.e., flaps, ailerons, tabs, etc. These may not be the best sources of control force at high frequency; loudspeakers, for example, may be better. Although they are usually regarded as weak load generators, when the area over which their influence is experienced is large, they generate very large and useful forces. That has been proved by the theoretical analysis and experiments described previously. Of course there are other acoustic devices that can be used as control force actuators. For example, a vibrating inertial mass mounted in the wing will cause a reaction force on the wing. We have conducted an experiment to show that such an internally mounted vibrator also gives good control performance.

Our experimental results show that the control could be switched on at will, but not from a very large amplitude. There is a moral here: if the control is always on, then large amplitudes will not arise and the controller will not be called upon to do much work. Disturbances in the air will, of course, place a natural limit on this relief because the system must respond linearly to those disturbances.

The present experiments were very easy to setup in the laboratory, and this leads us to expect that the principle and ideas we describe are quite robust. They might even form the basis for useful new technology.

Appendix

Two-Dimensional Line Source

We derive the Green function for the two-dimensional problem of a line source above a rigid strip of width 2b, shown in Fig. A1. In the low-frequency limit or for an incompressible medium, the equation for the pressure field in this situation is

$$\left(\frac{\partial^2}{\partial x^2}+\frac{\partial^2}{\partial y^2}\right)G = -\delta(x-x_0)\delta(y-y_0), \qquad \left.\frac{\partial G}{\partial y}\right|_{\substack{y=0\\ |x|<b}} = 0 \tag{A1}$$

We take the plane in Fig. A1 as the z plane, where $z = x + iy$, and use the Joukowski transformation

$$z = \frac{b}{2}\left(z_1 + \frac{1}{z_1}\right) \tag{A2}$$

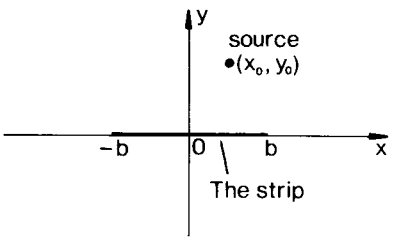

Fig. A1 The source relative to the strip.

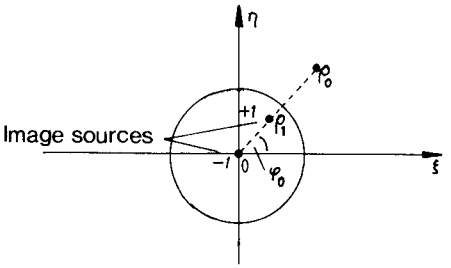

Fig. A2 The strip and source in the z_1 plane.

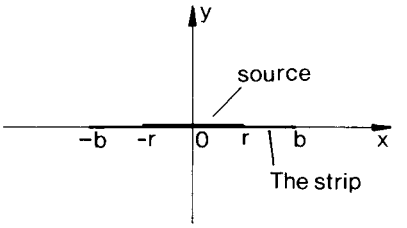

Fig. A3 A strip source embedded on the strip boundary surface.

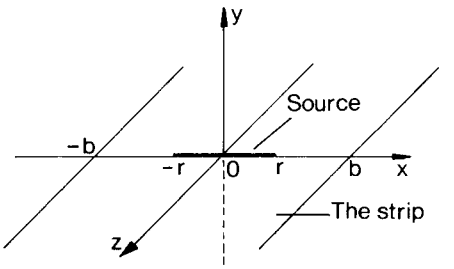

Fig. A4 Three-dimensional line source on the strip.

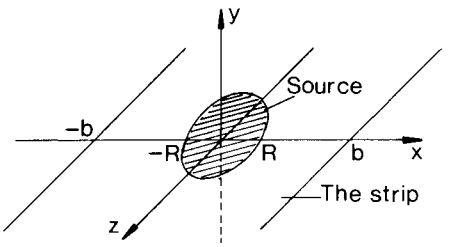

Fig. A5 Disk source on the strip.

where $z_1 = \xi + i\eta$. In polar coordinates $z_1 = \rho\cos\varphi + i\rho\sin\varphi$, Eq. (A1) can be written as

$$\left(\frac{\partial^2}{\partial\xi^2}+\frac{\partial^2}{\partial\eta^2}\right)G = -\delta(\xi-\xi_0)\delta(\eta-\eta_0), \qquad \left.\frac{\partial G}{\partial\rho}\right|_{\rho=1}=0 \tag{A3}$$

According to Eq. (A2), the source in the z_1 plane becomes (φ_0,ρ_0), and the strip becomes the unit circle. All of the z plane maps into the outside of the unit circle in the z_1 plane, as shown in Fig. A2. To meet the boundary condition of Eq. (A3), we use the image method and introduce two image sources: $+1(\varphi_0,\rho_1)$ and $-1(0,0)$, where $\rho_1 = 1/\rho_0$. The solution of Eq. (A3) is then written as

$$G(\varphi,\rho\,|\varphi_0,\rho_0) = -\frac{1}{4\pi}\{\ell n[\rho^2+\rho_0^2-2\rho\rho_0\cos(\varphi-\varphi_0)]$$

$$+\ell n[\rho^2\rho_0^2+1-2\rho\rho_0\cos(\varphi-\varphi_0)]-2\ell n\rho-2\ell n\rho_0\} \tag{A4}$$

In the z_1 plane, the force on the strip is

$$F = b\int_0^{2\pi} G(\varphi,\rho=1)\sin\varphi\,d\varphi \tag{A5}$$

Now we take the position of the source in the z plane as $(x_0=0, y_0=a)$, i.e., $[\varphi_0=\pi/2,\ \rho_0=a/b+\sqrt{1+(a/b)^2}]$ in the z_1 plane. Substituting Eq. (A4) into Eq. (A5) we get

$$F = bJ/(1+\sqrt{1-J^2}) \tag{A6}$$

where

$$J = (\epsilon+\sqrt{1+\epsilon^2})/(1+\epsilon^2+\epsilon\sqrt{1+\epsilon^2}), \qquad \epsilon = a/b$$

The asymptotic behavior of Eq. (A6) as $\epsilon\to 0$ and $\epsilon\to\infty$ are

$$F/b \underset{\epsilon\to 0}{\simeq} 1-\epsilon \tag{A7}$$

$$F/b \underset{\epsilon\to\infty}{\simeq} 1/(2\epsilon) \tag{A8}$$

Two-Dimensional Strip Source

A strip source, $2r$ in width embedded in the center of the strip boundary surface and $2b$ in width, $r<b$, is shown in Fig. 3A. In this case, the equation for the pressure field is

$$\left(\frac{\partial^2}{\partial x^2}+\frac{\partial^2}{\partial y^2}\right)p = -\Pi(x)\delta(y), \qquad \left.\frac{\partial p}{\partial y}\right|_{\substack{y=0\\ |x|<b}}=0 \tag{A9}$$

where

$$\Pi(x) = \Pi_0 \qquad |x|\le r$$
$$= 0 \qquad |x|>r$$

The pressure follows easily:

$$P(x,y) = \int \Pi(x_0)\delta(y_0)G(x,y\,|x_0,y_0)\,dx_0\,dy_0$$

$$= \int_{-r}^{r} \Pi_0 G(x,y\,|x_0,0)\,dx_0$$

where G is the Green function defined in Eq. (A4). Hence

$$p = \Pi_0 b\int_{\theta}^{\pi-\theta} G(\varphi,\rho\,|\varphi_0,1)\sin\varphi_0\,d\varphi_0$$

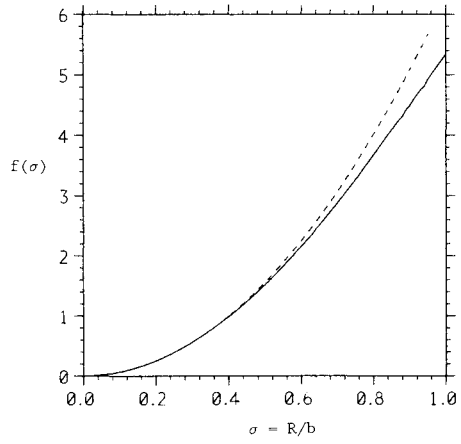

Fig. A6 Curves of function $f(\sigma)$ defined in Eq. (A16), in which the force induced by a disk source on the strip is $F=1/2\Pi_0 b^3(\sigma)$. —— $f(\sigma)$; ---- asymptotic form of $f(\sigma)$ as $\sigma \ll 1$.

where $\theta=\arccos(r/b)$. The force on the boundary is therefore

$$F=b\int_0^{2\pi} p(\varphi,1)\sin\varphi \mathrm{d}\varphi$$

$$=\Pi_0 b\int_0^{2\pi}\int_\theta^{\pi-\theta} G(\varphi,1)\sin\varphi\sin\varphi_0 \mathrm{d}\varphi\mathrm{d}\varphi_0$$

$$=\frac{1}{2}\Pi_0 b^2[\pi-2\arccos(r/b)+2(r/b)\sqrt{1-(r/b)^2}] \quad \text{(A10)}$$

Three-Dimensional Line Source

The situation is shown in Fig. A4. Equation (A9) becomes

$$\left(\frac{\partial^2}{\partial x^2}+\frac{\partial^2}{\partial y^2}+\frac{\partial^2}{\partial z^2}\right)p=-\Pi(x)\delta(y)\delta(z), \qquad \left.\frac{\partial p}{\partial y}\right|_{\substack{y=0\\|x|<b}}=0 \quad \text{(A11)}$$

Taking a Fourier transformation in z,

$$p(x,y,z)=\frac{1}{2\pi}\int_{-\infty}^{\infty}\hat{p}(x,y,k_z)e^{ik}z^z\mathrm{d}k_z$$

$$\hat{p}(x,y,k_z)=\int_{-\infty}^{\infty} pe^{-ik}z^z\mathrm{d}z$$

Eq. (A11) then becomes

$$\left(\frac{\partial^2}{\partial x^2}+\frac{\partial^2}{\partial y^2}\right)\hat{p}-k_z^2\hat{p}=-\Pi(x)\delta(y), \qquad \left.\frac{\partial\hat{p}}{\partial y}\right|_{\substack{y=0\\|x|<b}}=0 \quad \text{(A12)}$$

since the force on the strip is

$$F=\oint_{\text{strip}}\mathrm{d}x\int_{-\infty}^{\infty}p(x,0,z)\mathrm{d}z \quad \text{and} \quad F=\oint_{\text{strip}}\hat{p}(x,0,0)\mathrm{d}x$$

Setting $k_z=0$ in Eq. (A12) and using Eq. (A10), we can get the force directly:

$$F=1/2\Pi_0 b^2[\pi-2\arccos(r/b)+2(r/b)\sqrt{1-(r/b)^2}] \quad \text{(A13)}$$

Three-Dimensional Disk Source

A disk source is shown in Fig. A5. The governing equation of the pressure is

$$\left(\frac{\partial^2}{\partial x^2}+\frac{\partial^2}{\partial y^2}+\frac{\partial^2}{\partial z^2}\right)p=-\Pi(x,z)\delta(y), \qquad \left.\frac{\partial p}{\partial y}\right|_{\substack{y=0\\|x|<b}}=0 \quad \text{(A14)}$$

where

$$\Pi(x,z)=\Pi_0 \qquad \sqrt{x^2+z^2}\le R$$

$$=0, \qquad \sqrt{x^2+z^2}>R$$

The disk source can be divided into strips parallel to the x axis. According to the preceding analysis, each strip, being $2\sqrt{R^2-z^2}$ in length and dz in width, contributes a force of

$$\mathrm{d}F=1/2\Pi_0 b^2\mathrm{d}z[\pi 2-\arccos\sqrt{(R^2-z^2)/b^2}$$
$$+2\sqrt{(R^2-z^2)/b^2}\sqrt{1-(R^2-z^2)/b^2}]$$

Thus the total force is

$$F=\int_{-R}^{R}\mathrm{d}F$$

$$=1/2\Pi_0 b^2\int_{-R}^{R}[\pi-2\arccos\sqrt{(R^2-z^2)/b^2}$$
$$+2\sqrt{(R^2-z^2)/b^2}\sqrt{1-(R^2-z^2)/b^2}]\mathrm{d}z \quad \text{(A15)}$$

Setting $\xi=z/b$, $\sigma=R/b$, and $0\le\sigma\le 1$, Eq. (A15) becomes

$$F=1/2\Pi_0 b^3 f(\sigma) \quad \text{(A16)}$$

where

$$f(\sigma)=\int_{-\sigma}^{\sigma}[\pi-2\arccos\sqrt{\sigma^2-\xi^2}+2\sqrt{\sigma^2-\xi^2}\sqrt{1-(\sigma^2-\xi^2)}]\mathrm{d}\xi$$

$$=4\int_0^{\pi/2}(\sigma^2-\sigma^4\sin^4\theta)/\sqrt{1-\sigma^2\sin^2\theta}\mathrm{d}\theta$$

In the case of $\sigma\ll 1$,

$$f(\sigma)\simeq 4\int_0^{\pi/2}\sigma^2\mathrm{d}\theta=2\pi\sigma^2=2\pi\left(\frac{R}{b}\right)^2$$

so that Eq. (A16) can be written as

$$F\simeq\pi\Pi_0 bR^2, \qquad (R/b\ll 1) \quad \text{(A17)}$$

$f(\sigma)$ and its asympototic form are plotted in Fig. A6. From Fig. A6 we can see that when $R/b<0.5$, the two curves are nearly coincidental.

A piston oscillating with normal displacement $\zeta=\zeta_0 e^{i\omega t}$ can be considered as the disk source. In that case, $\Pi_0=-\omega^2\rho_0\zeta$, and the force on the strip will be

$$F=-\tfrac{1}{2}\rho_0\omega^2 b^3\zeta f(\sigma) \quad \text{(A18a)}$$

or

$$F=-\pi\rho_0\omega^2 bR^2\zeta, \qquad (R/b<0.5) \quad \text{(A18b)}$$

where ρ_0 is air density.

Disk Source Above the Strip

If the strength of the disk source above the strip is $\Pi(x,z)$ and the distance from the source to the strip is a, then the force on the strip is

$$F=\int\Pi(x_0,z_0)G(x,0,z\,|x_0,a,z_0)\mathrm{d}x\mathrm{d}z\mathrm{d}x_0\mathrm{d}z_0 \qquad \text{(A19)}$$

where G is the Green function. In the case of the radius of disk $R \ll b$, we can set

$$G(x,y,z\,|x_0,a,z_0)\simeq G(x,y,z\,|0,a,0)$$

and following the preceding analysis, we find that

$$\int G(x,0,z\,|x_0,a,z_0)\mathrm{d}x\mathrm{d}z\simeq\int G(x,0,z\,|0,a,0)\mathrm{d}x\mathrm{d}z$$

$$=bJ/(1+\sqrt{1-J^2})$$

where

$$J=(\epsilon+\sqrt{1+\epsilon^2})/(1+\epsilon^2+\sqrt{1+\epsilon^2}),\quad \epsilon=a/b$$

Equation (A19) then becomes

$$F=bJ/(1+\sqrt{1-J^2})\int\Pi(x_0,z_0)\mathrm{d}x_0\mathrm{d}z_0$$

For a piston, $\Pi(x_0,z_0)=-\rho_0\omega^2\zeta$ and $x_0^2+z_0^2\le R$; therefore,

$$F=-\rho_0\omega^2\pi R^2\zeta\alpha \qquad \text{(A20)}$$

where ζ is the normal displacement of the piston and $\alpha=bJ/(1+\sqrt{1-J^2})$.

Acknowledgments

This work is part of the author's postgraduate studies under the supervision of Professor J. E. Ffowcs Williams. I am grateful for his guidance and for the financical support of University of Cambridge and Academia Sinica, which made my study at Cambridge possible. Thanks must also go to Mr. R. G. Carter for his technical assistance and Mr. D. C. Hill for his help in preparing this paper.

References

[1]Thompson, G. O. and Kass, G. J., "Active Flutter Suppression—An Emerging Technology," *Proceedings of the Joint Automatic Control Conference*, 1971, pp. 608–616.

[2]Noll, T. E. and Felt, L. R., "Active Flutter Suppression—A Practical Application," *Proceedings of the National Aerospace Electronics Conference*, IEEE, 1973, pp.329–334.

[3]Abel, I., Perry, B., and Mirrow, H. H., "Synthesis of Active Controls for Flutter Suppression on Flight Research Wing," NASA 77-1062, 1977.

[4]Johnson, E. H., "Active Flutter Suppression Control Law Definition via Least Square Synthesis," *Proceedings of the AIAA/ASME/ASCE/AHS 21st Structures, Structural Dynamics, and Material Conference*, Seattle, WA, 1980, pp. 595–609.

[5]Nissim, E., "Flutter Suppression Using Active Control Based on the Concept of Aerodynamic Energy, NASA TN-6199, 1971.

[6]Sandford, M. C., Abel, I., and Gray D. L., "Development and Demonstration of a Flutter—Suppression System Using Active Controls," NASA TR R-450, 1975.

[7]Ffowcs Williams, J. E., "Anti-Sound," *Proceedings of the Royal Society of London*, Series A 395, 1984, pp. 63–88.

[8]Morse, P. M. and Ingard, K. U., "Theoretical Acoustics," McGraw-Hill, New York, 1968, pp. 383–384.